

Supplementary Information

Strategic weakening for holistic strengthening: overstrain-driven synchronous strengthening-toughening in sustainable rubber via “weak” non-covalent networks

Wei-Chen Zhou^{1, 2, 3}, Xue-Qin Gao^{1, 3*}, Jia-Hao Li^{1, 2, 3}, Yan Wang^{2, 5}, Yu-Zhong Wang^{1, 2, 5}, and Cong Deng^{2, 4*}

1- State Key Laboratory of Advanced Polymer Materials, Sichuan University, Chengdu 610065, People's Republic of China

2- Collaborative Innovation Center for Eco-Friendly and Fire-Safety Polymeric Materials (MoE), National Engineering Laboratory for Eco-Friendly Polymer Materials (Sichuan), Sichuan University, Chengdu 610064, People's Republic of China

3- College of Polymer Science and Engineering, Sichuan University, Chengdu 610065, People's Republic of China

4- Analytical & Testing Center, Sichuan University, Chengdu 610064, People's Republic of China

5- College of Chemistry, Sichuan University, Chengdu 610064, People's Republic of China

E-mail addresses: dengcong@scu.edu.cn (C. Deng), gaoxueqin@scu.edu.cn (X.-Q. Gao)

Materials

ENR-50 (epoxidation degree of 50%, $M_n=100178$, polymer dispersity index=2.196) was purchased from the Agricultural Products Processing Research Institute, China. 2-Amino-4-hydroxy-6-methylpyrimidine (UPy, 98%), hexamethylene diisocyanate (HDI, 98%), 4-aminobenzoic acid (ABA, 98%), N-Acetylglycine (AG, 99%), Zinc acetate dihydrate ($Zn(OAc)_2 \cdot 2H_2O$, 99.99%) and 1,2-dimethylimidazole (DMI, 98%) were purchased from Aladdin Ltd, China. Cyclohexane (CYH, 99%), trichloromethane (TCM, 99%) and anhydrous ethanol (EtOH, 99%) were purchased from Kelong Co., Ltd, China.

Prepare of ENR Containing Non-Covalent Networks

ENR-50 was blended with precise amounts of NAg, UPy-COOH, $Zn(OAc)_2 \cdot 2H_2O$, and DMI using a two-roll mill. The resulting mixture was then left undisturbed for 24 hours before undergoing vulcanization in a flat vulcanizing press. The process was conducted at a temperature of 180°C and a pressure of 10 MPa, with the vulcanization duration determined based on the corresponding vulcanization curve. DMI, functioning as a catalyst to facilitate the reaction between epoxy groups and carboxyl moieties^{1, 2}, was incorporated in an equimolar proportion relative to the carboxyl groups.

Characterizations

Nuclear magnetic resonance (¹H NMR) spectroscopy was conducted using a Bruker AVANCE III HD-400 spectrometer (Bruker, Germany), with deuterated DMSO-d₆ as the solvent and tetramethylsilane (TMS) as the internal reference. Thermogravimetric analysis (TGA) was conducted on a TG 209F1 thermogravimetric analyzer (NETZSCH, Germany) over a temperature range of 40–700 °C, with a heating rate of 10 °C/min under a nitrogen atmosphere at a flow rate of 50 mL/min. Fourier-transform infrared (FTIR) spectroscopy was performed on a Nicolet 6700 spectrometer (Thermo Fisher Scientific, USA) using the KBr pellet method for transmission analysis. The rubber's structural characteristics were further examined through attenuated total reflection (ATR) spectroscopy, covering a wavenumber range of 400–4000 cm⁻¹. The

vulcanization behavior of the rubber was assessed with an RPA8000 rubber processing analyzer (GOTECH, Taiwan) at 180 °C. Rheological properties were measured using a Discovery HR-2 Dynamic Rheometer (TA Instruments, USA) at 25 °C. Circular specimens (25 mm in diameter, 1 mm thick) were subjected to strain sweep tests at a shear rate of 1 Hz and frequency sweep tests at a shear strain of 1%. Dynamic mechanical analysis (DMA) and stress relaxation studies were performed on a Q850 dynamic mechanical analyzer (TA Instruments, USA) in tensile mode, using samples with a thickness of 0.5 mm. Fitting the $\ln(\tau)$ versus $1/T$ for the samples exhibited a linear temperature dependence consistent with the Arrhenius equation:

$$\ln \tau(T) = \ln \tau_0 + \frac{E_a}{RT}$$

where τ_0 represents the relaxation time at infinite temperature, R is the gas constant ($8.314 \text{ J}\cdot\text{mol}^{-1}\cdot\text{K}^{-1}$), and E_a denotes the apparent activation energy governing the relaxation behavior. Testing parameters included a frequency of 1 Hz, an amplitude of $15 \mu\text{m}$, and a temperature range of -50 - $100 \text{ }^\circ\text{C}$ at a heating rate of $3 \text{ }^\circ\text{C}/\text{min}$. Stress relaxation behavior was analyzed under a constant strain of 3%. Mechanical properties were examined at room temperature using an INSTRON 3366 universal testing machine (Instron Limited, USA) in accordance with GB/T 528-2009 standards. A 1 kN load cell was utilized, with tensile testing performed at a rate of $500 \text{ mm}\cdot\text{min}^{-1}$. Dumbbell-shaped specimens (18 mm in length, 4 mm in width, and 1 mm in thickness) were used for testing. Cyclic tensile tests were conducted under identical conditions, with the tensile rate adjusted to $100 \text{ mm}\cdot\text{min}^{-1}$. The tensile toughness of the specimens is determined by calculating the integral of the area beneath the stress-strain curves. True stress and true strain are derived from the engineering stress-strain data using the following equation³:

$$\sigma_{ture} = \sigma \cdot (\varepsilon + 1) ; \varepsilon_{ture} = \ln(\varepsilon + 1)$$

The Mooney stress f^* and elongation ratio λ were fitted according to the formula⁴:

$$f^* = \frac{\sigma}{\lambda - \lambda^{-2}} = 2C_1 + 2C_2\lambda^{-1}$$

where σ is the tensile stress, and C_1 and C_2 are material constants.

Reprocessability experiments were carried out following established literature protocols⁵. To enhance flowability during processing, the cured rubber was reprocessed by blending it with 20% uncrosslinked rubber. The resulting mixture was then vulcanized using a flat-plate vulcanizer under the same curing conditions as the initial vulcanization. Small-angle X-ray scattering (SAXS) measurements were performed using a Xeuss 2.0 SAXS system, with a Cu target serving as the X-ray source. The sample-to-detector distance was set at 1300 mm, and the exposure duration was fixed at five minutes.

Density Functional Theory (DFT) Calculations

DFT computations were performed utilizing the Gaussian 09 software package⁶. Geometry optimizations were conducted at the B3LYP/def2-SVP level, incorporating D3BJ⁷⁻⁹ dispersion corrections. To verify that each optimized structure corresponded to a true energy minimum, vibrational frequency analyses were carried out. Solvent effects were accounted for using the IEFPCM model, with water as the simulated medium. Subsequently, single-point energy calculations were performed on the optimized geometries at the B3LYP/def2-TZVP level, also including D3BJ dispersion corrections, to obtain accurate energy estimates.

All-Atom Molecular Dynamics (MD) Simulations

MD simulations were conducted using the Materials Studio software package. Initially, fundamental molecular units m, n, o, and p were constructed based on their molecular structures (**Fig. 1A**). These units were then subjected to structural optimization using the COMPASS force field, yielding stable configurations. Subsequently, single chains were constructed from the m, n, o, and p molecular units following the methodology outlined in the references. These single-chain structures were further optimized to obtain their most stable conformations. Building upon the optimized single-chain structures, a polymer structure with a density of 0.96 g/cm³ was generated. The obtained polymeric system first underwent energy minimization to achieve a stable configuration. Following this, a 50 ps relaxation was performed in the NPT ensemble

using the COMPASS force field to further stabilize the structure. Finally, molecular dynamics (MD) simulations were carried out in the NVT ensemble at room temperature, employing a 0.2 fs time step for 100 ps. During the simulation, structural configurations were recorded at 0.5 ps intervals, resulting in a total of 200 frames. The cohesive energy density for each frame was computed according to established literature protocols³, and the final value was obtained by averaging across all frames.

Supplementary Figures

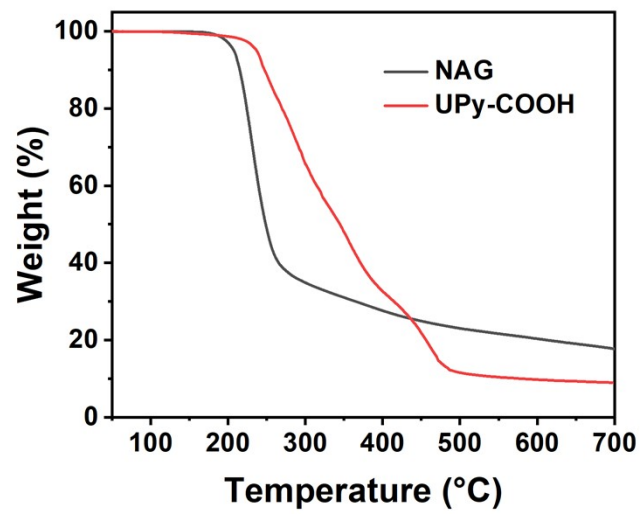


Fig. S1 The TG curves of NAG and UPy-COOH.

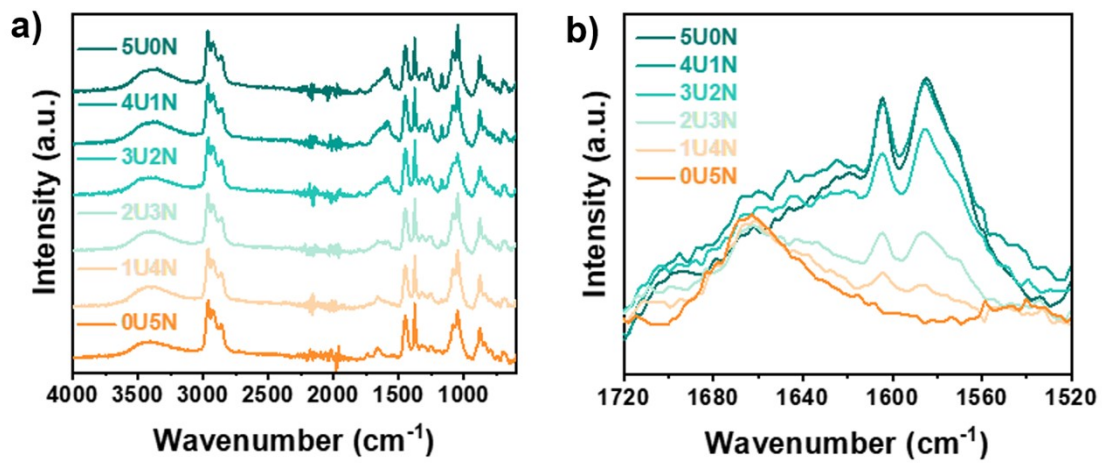


Fig. S2 The FTIR spectra of xUyN.

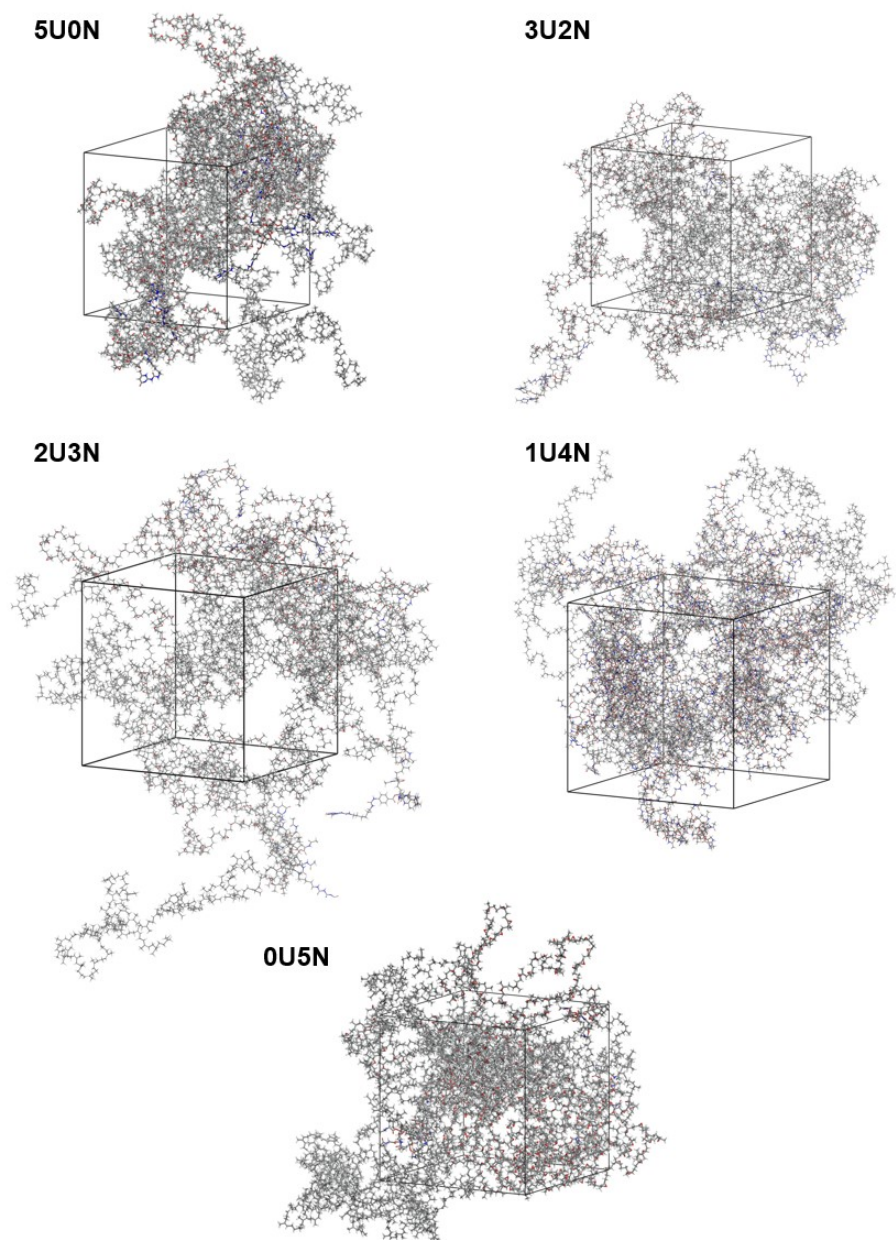


Fig. S3 The structure of the MD simulations of $xUyN$.

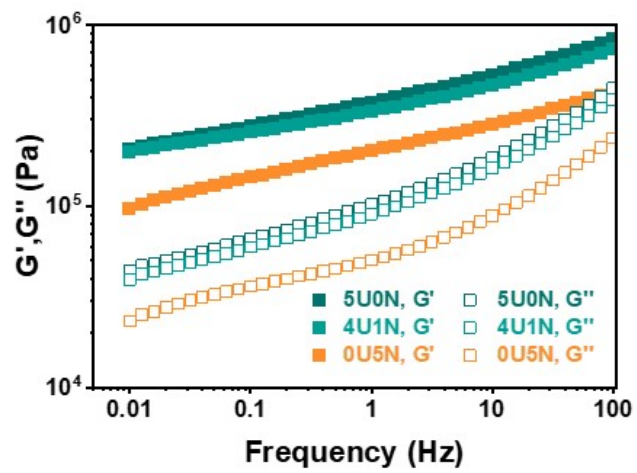


Fig. S4 The frequency sweep curves of xUyN.

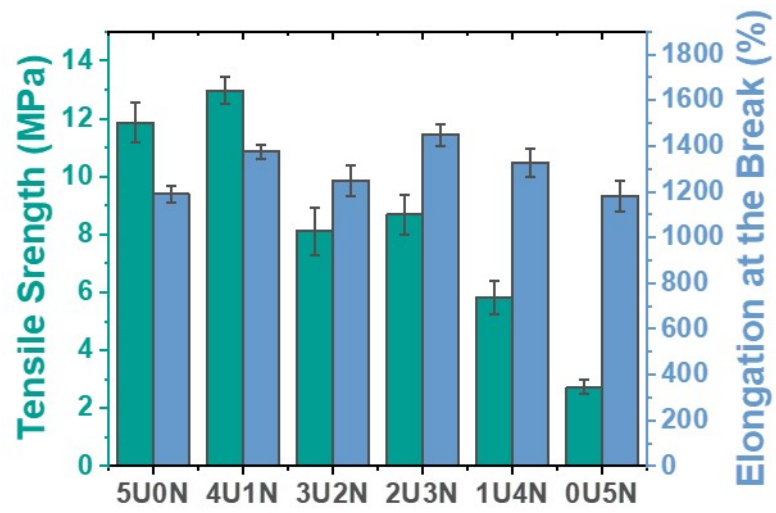


Fig. S5 The mechanical properties of $xUyN$.

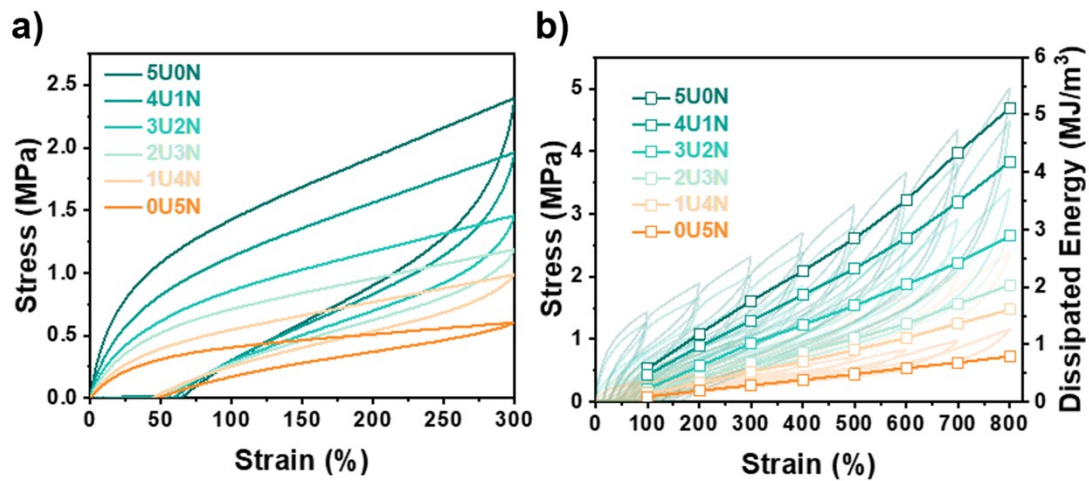


Fig. S6 a) The cyclic tensile curves of xUyN. b) The cyclic tensile curves of xUyN with multiple consecutive increments.

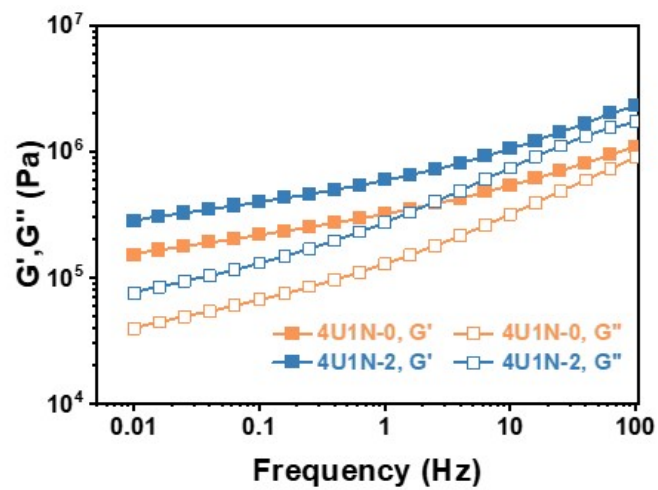


Fig. S7 The frequency sweep curves of 4U1N and 4U1N-2.

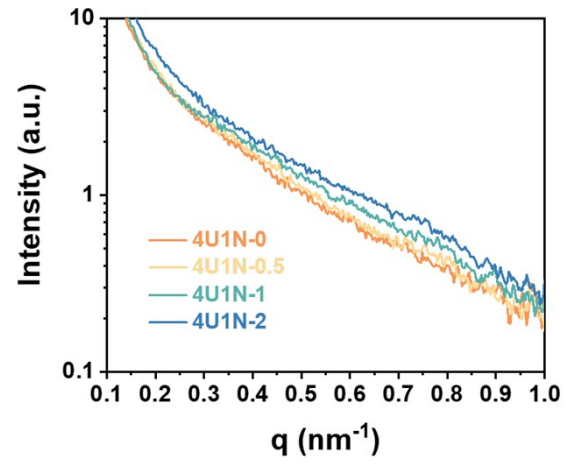


Fig. S8 The I- q curves of 4U1N- x .

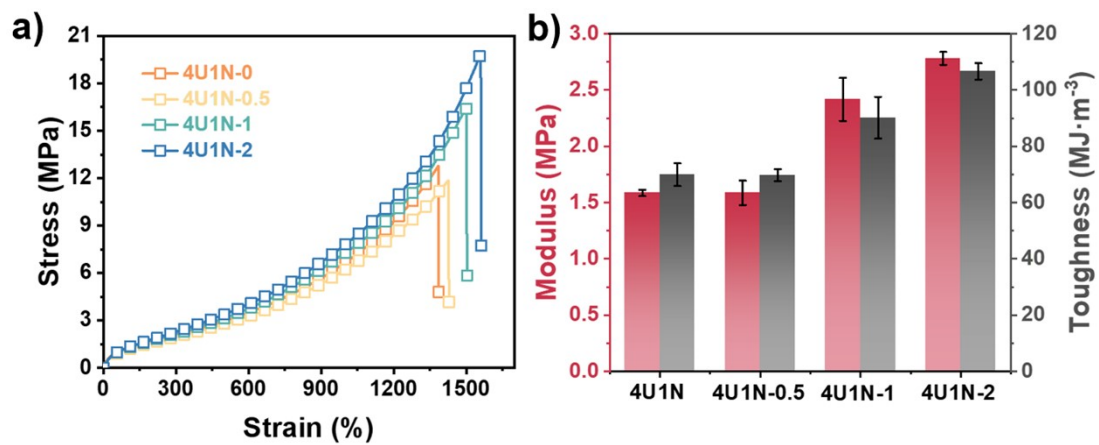


Fig. S9 a) The stress-strain curves of 4U1N-x. b) The modulus and toughness of 4U1N-x.

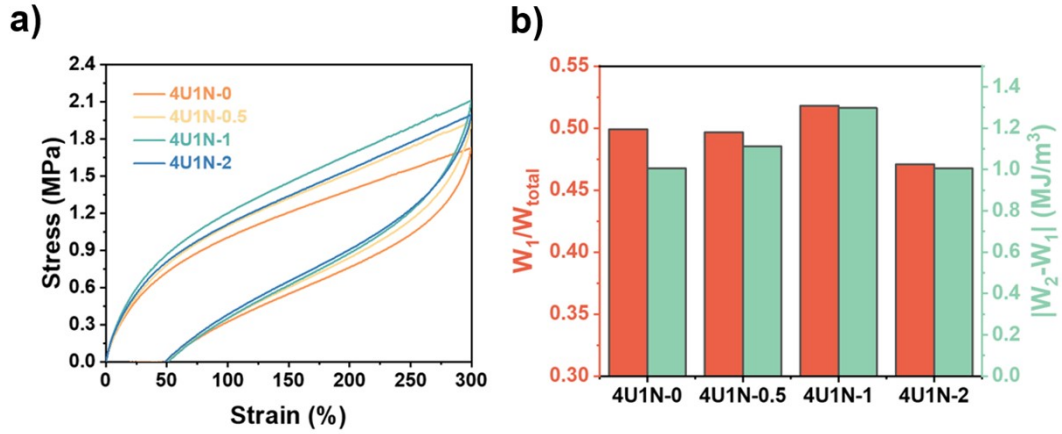


Fig. S11 a) The cyclic tensile curves of 4U1N-x. b) The energy dissipation efficiency and energy dissipation variation of 4U1N-x.

To quantitatively assess the energy dissipation capacity of 4U1N-x, we introduced two key physical parameters: energy dissipation efficiency and energy dissipation variation. Energy dissipation efficiency is defined as the ratio of the hysteresis loop area from the initial loading-unloading cycle (W_1) to the total area under the loading curve (W_{total}), expressed as W_1/W_{total} . Meanwhile, energy dissipation variation is characterized by the absolute difference between the hysteresis loop areas of the second (W_2) and first (W_1) loading-unloading cycles, represented as $|W_2 - W_1|$.

The relatively lower energy dissipation in 4U1N-2 may result from the interplay between hydrogen bonding and Zn^{2+} -O coordination. At low Zn^{2+} content, the weaker coordination allows bond dissociation under strain, thereby enhancing energy dissipation. However, as Zn^{2+} content increases, the cohesive energy density also increases, making it harder for the coordination bonds to break at the same strain level. Furthermore, Zn^{2+} inhibits the formation of UPy-based quadruple hydrogen bonds (as shown in Fig. 3d), which also contribute to reduced energy dissipation. Consequently, the net dissipation efficiency of 4U1N-2 is lower than in other samples.

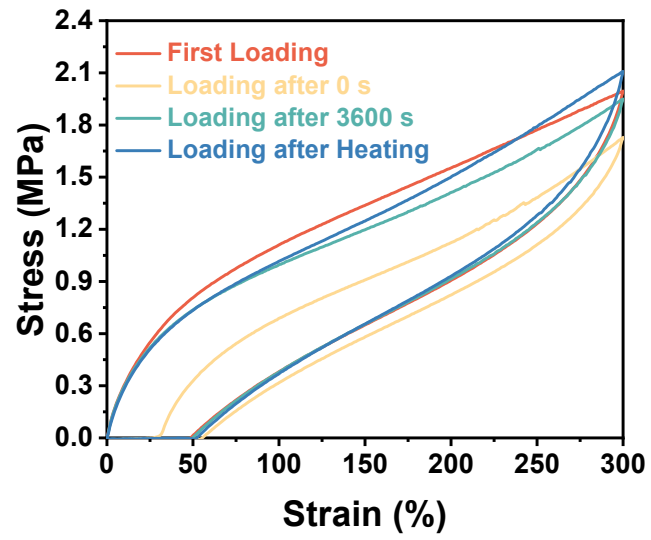


Fig. S12 The cyclic tensile curves of 4U1N-2 after different time and thermal treating at 80 °C for 15 minutes.

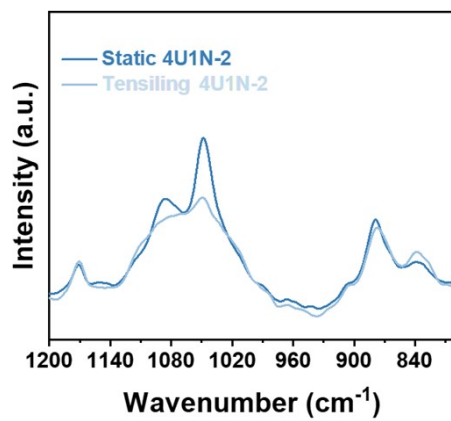


Fig. S13 The FTIR spectra of static and tensiling 4U1N-2.

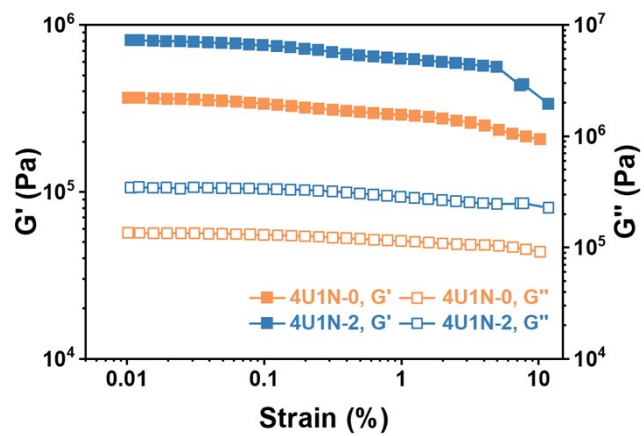


Fig. S14 The strain sweep curves of 4U1N and 4U1N-2.

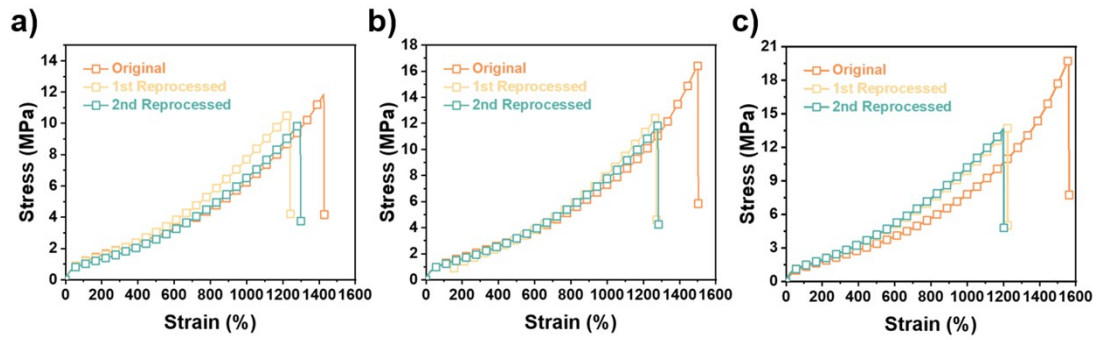


Fig. S15 The stress-strain curves of a) 4U1N-0.5, b) 4U1N-1 and c) 4U1N-2 before and after reprocessing.

Based on our prior research¹⁰, we attribute the reduced reprocessing efficiency to partial consumption of epoxy groups during repeated processing in the presence of moisture and acetate ions. This variation leads to a reduction in the density of Zn^{2+} coordination sites, thereby weakening the cohesive strength of the reprocessed material.

Nevertheless, the rational design of non-covalent networks ensures that even after two reprocessing cycles, 4U1N-2 retains superior absolute mechanical performance compared to the original values reported for other reprocessable rubbers.

Supplementary Tables

Table S1 Mechanical properties of xUyN.

Samples	Young's Modulus (MPa)	Tensile Strength (MPa)	Elongation at the Break (%)	Toughness (MJ/m³)
5U0N	1.67±0.09	11.87±0.71	1190±38	62.00±4.49
4U1N	1.59±0.03	12.96±0.47	1377±31	69.95±4.01
3U2N	1.09±0.12	8.11±0.82	1248±66	43.45±5.24
2U3N	1.17±0.10	8.69±0.67	1448±47	48.97±4.74
1U4N	0.71±0.09	5.81±0.58	1329±63	30.82±5.28
0U5N	0.33±0.01	2.72±0.24	1182±68	15.44±2.30

Table S2 Mechanical properties of 4U1N-x.

Samples	Young's Modulus (MPa)	Tensile Strength (MPa)	Elongation at the Break (%)	Toughness (MJ/m³)
4U1N	1.59±0.03	12.96±0.47	1377±31	69.95±4.01
4U1N-0.5	1.59±0.11	12.29±1.15	1424±44	69.72±2.15
4U1N-1	2.42±0.19	16.56±0.54	1528±33	90.18±7.41
4U1N-2	2.78±0.06	19.36±0.65	1529±35	106.67±2.90

Table S3 Comparison of the mechanical properties between this work and other reprocessable rubbers.

Network	Strength (MPa)	Elongation at Break (%)	Toughness (MJ/m³)	Ref
Covalent Adaptive Networks (CANs)	2.68	215	/	11
	1.9	315		12
	1.16	53		13
	14.63	475		14
	3.1	583		15
	2.62	739	10.31	16
	21.4	284.1	~30	17
	22.3	147.2		18
	19.44	886		19
	~1.5	~155		20
CANs with Sacrificial Bonds	25.7	421	43.1	21
	3	208	3.15	22
	14.6	505	38.1	23
	21.4	447	36.8	24
	16.56	776	56.9	25
	27.97	493	40.2	26
	13.7	174		27
CANs with Fillers	7.26	596		28
	4.5	400		29
	16.1	299	47.2	30
	19.4	158		31

	21.11	199		32
	22	380		33
	9.9	226		34
	14.1	188		35
	4.95	130		36
Non-Covalent Interactions	8.57	793	39.12	37
	3.6	271		38
	~2.7	~360		39
	18.18	927	74.34	10
	19.36	1529	106.67	Our Work

Table S4 Comparison of the mechanical properties after reprocessing of rubbers between this work and other reprocessable rubbers.

Network	Strength (MPa)	Elongation at Break (%)	Ref
Covalent Adaptive Networks (CANs)	~2.5	~200	11
	~1.8	~200	12
	~1.4	~60	13
	~12	~400	14
	~1.1	~500	15
	~2.7	~850	16
	~21	~270	17
	~16	~150	18
	~20	~800	19
	~1.2	~100	20
CANs with Sacrificial Bonds	~15	~300	21
	~3	~208	22
	~10	~650	23
	~15	~400	24
	~15	~600	25
	~16	~450	26
	~7	~150	27
CANs with Fillers	~5	~700	28
	~4.5	~400	29
	~16	~200	30
	~12	~250	31

	~20	~200	32
	~12	~380	33
	~6	~200	34
	~13	~150	35
	4.76	182	36
Non-Covalent Interactions	~8	~700	37
	~2	~600	38
	~3	~160	39
	11.84	954	10
	13.64	1199	Our Work

References

1. M. Pire, S. Norvez, I. Iliopoulos, B. Le Rossignol and L. Leibler, *Polymer*, 2011, **52**, 5243-5249.
2. M. Pire, C. Lorthioir, E. K. Oikonomou, S. Norvez, I. Iliopoulos, B. Le Rossignol and L. Leibler, *Polymer Chemistry*, 2012, **3**, 946-953.
3. Z. Li, Y.-L. Zhu, W. Niu, X. Yang, Z. Jiang, Z.-Y. Lu, X. Liu and J. Sun, *Advanced Materials*, 2021, **33**, 2101498.
4. L. Bokobza and B. Erman, *Macromolecules*, 2000, **33**, 8858-8864.
5. W. Song, Z. Wang, Y. Xing, G. Zhang, X. Zhang, Y. Lu, T. Tan and L. Zhang, *ACS Sustainable Chemistry & Engineering*, 2023, **11**, 2784-2796.
6. G. W. T. M. J. Frisch, H. B. Schlegel, G. E. Scuseria, M. A. Robb, J. R. Cheeseman, G. Scalmani, V. Barone, B. Mennucci, G. A. Petersson, H. Nakatsuji, M. Caricato, X. Li, H. P. Hratchian, A. F. Izmaylov, J. Bloino, G. Zheng, J. L. Sonnenberg, M. Hada, M. Ehara, K. Toyota, R. Fukuda, J. Hasegawa, M. Ishida, T. Nakajima, Y. Honda, O. Kitao, H. Nakai, T. Vreven, J. A. Montgomery, Jr., J. E. Peralta, F. Ogliaro, M. Bearpark, J. J. Heyd, E. Brothers, K. N. Kudin, V. N. Staroverov, T. Keith, R. Kobayashi, J. Normand, K. Raghavachari, A. Rendell, J. C. Burant, S. S. Iyengar, J. Tomasi, M. Cossi, N. Rega, J. M. Millam, M. Klene, J. E. Knox, J. B. Cross, V. Bakken, C. Adamo, J. Jaramillo, R. Gomperts, R. E. Stratmann, O. Yazyev, A. J. Austin, R. Cammi, C. Pomelli, J. W. Ochterski, R. L. Martin, K. Morokuma, V. G. Zakrzewski, G. A. Voth, P. Salvador, J. J. Dannenberg, S. Dapprich, A. D. Daniels, O. Farkas, J. B. Foresman, J. V. Ortiz, J. Cioslowski, D. J. Fox, Gaussian 09, Version D.01, Gaussian, Inc., Wallingford CT, 2013., *Journal*.
7. F. Weigend and R. Ahlrichs, *Physical Chemistry Chemical Physics*, 2005, **7**, 3297-3305.
8. S. Grimme, J. Antony, S. Ehrlich and H. Krieg, *The Journal of Chemical Physics*, 2010, **132**, 154104.
9. S. Grimme, S. Ehrlich and L. Goerigk, *Journal of Computational Chemistry*, 2011, **32**, 1456-1465.
10. W.-C. Zhou, X.-Q. Gao, J.-H. Li, C. Ye, Y.-Z. Wang and C. Deng, *Journal of Materials Chemistry A*, 2025, **13**, 1746-1754.
11. Y. Chen, Z. Tang, X. Zhang, Y. Liu, S. Wu and B. Guo, *ACS Applied Materials & Interfaces*, 2018, **10**, 24224-24231.
12. X. Li, S. Wu, S. Yu, C. Xiao, Z. Tang and B. Guo, *Polymer*, 2022, **238**, 124379.
13. Y. Liu, Z. Tang, J. Chen, J. Xiong, D. Wang, S. Wang, S. Wu and B. Guo, *Polymer Chemistry*, 2020, **11**, 1348-1355.
14. Y. Chen, Z. Tang, Y. Liu, S. Wu and B. Guo, *Macromolecules*, 2019, **52**, 3805-3812.
15. W. Liu, J. Huang, Z. Gong, J. Fan and Y. Chen, *Polymer*, 2022, **252**, 124900.
16. J. Huang, Z. Gong and Y. Chen, *Polymer*, 2022, **242**, 124569.
17. J. Huang, X. Wang, H. Wu, S. Xiao, Y. Liang, H. Yu, B. Xu, W. Xu and L. Tan, *Chemical Engineering Journal*, 2024, **490**, 151516.
18. Y. Zou, Y.-F. Yao, R. Zhang, Y.-H. Zhao, J. Cao and Y.-X. Xu, *ACS Sustainable Chemistry & Engineering*, 2023, **11**, 18123-18130.
19. Y. Liu, M.-L. Wu, Y.-D. Li, L.-Y. Li and J.-B. Zeng, *ACS Sustainable Chemistry & Engineering*, 2023, **11**, 17190-17198.
20. H. Xiang, J. Yin, G. Lin, X. Liu, M. Rong and M. Zhang, *Chemical Engineering Journal*, 2019, **358**, 878-890.
21. Y. Liu, Z. Tang, D. Wang, S. Wu and B. Guo, *Journal of Materials Chemistry A*, 2019, **7**, 26867-26876.

22. L. Wang, Y. Liu, N. Hao, Y. Qiao, W. Zeng, L. Wei and A. Du, *Polymer*, 2023, **265**, 125595.
23. X. Qi, J. Zhang, L. Zhang and D. Yue, *Journal of Materials Chemistry A*, 2021, **9**, 25399-25407.
24. S. Wu, S. Fang, Z. Tang, F. Liu and B. Guo, *Materials & Design*, 2020, **192**, 108756.
25. L. Huang, Y. Yang, Z. Niu, R. Wu, W. Fan, Q. Dai, J. He and C. Bai, *Macromolecular Rapid Communications*, 2021, **42**, 2100432.
26. Y. Liu, Z. Tang, S. Wu and B. Guo, *ACS Macro Letters*, 2019, **8**, 193-199.
27. H. Dong, G. Zhang and Y. Zhang, *Composites Science and Technology*, 2023, **238**, 110025.
28. L. Cao, J. Fan, J. Huang and Y. Chen, *Journal of Materials Chemistry A*, 2019, **7**, 4922-4933.
29. C. Xu, R. Cui, L. Fu and B. Lin, *Composites Science and Technology*, 2018, **167**, 421-430.
30. L. Huang, Y. Yang, Z. Niu, R. Wu, W. Fan, Q. Dai, J. He and C. Bai, *Composites Science and Technology*, 2022, **228**, 109621.
31. S. Wu, Z. Yang, S. Fang, Z. Tang, F. Liu and B. Guo, *Journal of Materials Chemistry A*, 2019, **7**, 1459-1467.
32. M. Qiu, S. Wu, Z. Tang and B. Guo, *Composites Science and Technology*, 2018, **165**, 24-30.
33. Z. Tang, Y. Liu, B. Guo and L. Zhang, *Macromolecules*, 2017, **50**, 7584-7592.
34. Y. Liu, Z. Tang, Y. Chen, C. Zhang and B. Guo, *ACS Applied Materials & Interfaces*, 2018, **10**, 2992-3001.
35. G. Zhang, C. Tian, H. Chu, J. Liu, B. Guo and L. Zhang, *Journal of Materials Chemistry A*, 2023, **11**, 25356-25367.
36. J. Huang, L. Zhang, Z. Tang, S. Wu and B. Guo, *Composites Science and Technology*, 2018, **168**, 320-326.
37. W. Wang, W. Zhang, Z. Liu, Y. Xue, X. Lei, G. Gong and Q. Zhang, *Journal of Materials Chemistry C*, 2021, **9**, 6241-6250.
38. L. Cao, Z. Gong, C. Liu, J. Fan and Y. Chen, *Composites Science and Technology*, 2021, **207**, 108750.
39. C. Xu, J. Nie, W. Wu, Z. Zheng and Y. Chen, *ACS Sustainable Chemistry & Engineering*, 2019, **7**, 15778-15789.